Biologically influenced gas fluxes revealed by high-resolution monitoring of unsaturated soil columns

Clement Alibert, Eric Pili, Pierre Barre, Florent Massol, Simon Chollet

Received: 6 November 2019 | Accepted: 18 February 2020

DOI: 10.1002/vzj2.20018

Vadose Zone Journal

ORIGINAL RESEARCH ARTICLE

Biologically influenced gas fluxes revealed by high-resolution monitoring of unsaturated soil columns

Clement Alibert[1,2,3] | **Eric Pili**[1] | **Pierre Barre**[1] | **Florent Massol**[2] | **Simon Chollet**[2]

[1]Lab. de Géologie de l'ENS, PSL Research Univ., UMR8538, Paris, 75005 France

[2]CEREEP Ecotron-IDF, CNRS, UMS3194, Saint-Pierre-lès-Nemours, 77140 France

[3]CEA, DAM, DIF, Arpajon, F-91297 France

Correspondence
Clement Alibert, Lab. de Géologie de l'ENS, PSL Research Univ., UMR8538, 75005 Paris, France.
Email: clement.alibert@ens.psl.eu

Abstract

Modulations of advective gas fluxes at the soil–atmosphere interface were investigated using an enhanced experimental setup developed to perform tracer gas percolation experiments through unsaturated soil columns under well-controlled conditions associated with long-term and high-resolution monitoring. The setup design includes the effect of watering and evaporation cycles, barometric pressure fluctuations, variations in the injection pressure, and plant metabolism. Although injected at a constant flux at the base of the columns, SF_6 surface fluxes varied on a timescale of hours to days. These modulations are controlled by (a) barometric pressure, (b) water content and distribution, and (c) plant metabolism. All three mainly act on the pressure gradient. Surface gas fluxes decrease under drying conditions, which increases gas porosity and the relative gas permeability and lowers the pressure gradient. Respiration of plant roots is shown to be responsible for daytime–nighttime oscillations of the tracer flux. During nighttime, O_2 consumption and CO_2 production locally lowers the pressure gradient up to the root zone due to the higher solubility of CO_2 in pore water, resulting in an increased SF_6 flux at the surface. During daytime, enhanced water loss by evapotranspiration associated with photosynthesis dominated the respiration effect and resulted in decreasing surface gas fluxes, as generally shown for drying conditions. Surface gas fluxes are therefore controlled by combined physical, chemical, and biological processes. This has important consequences, notably when discrete flux measurements are integrated in space and/or in time to quantify emissions or when used for detecting, identifying, or monitoring underground gas sources.

1 | INTRODUCTION

Gas transport in soils is highly variable in space and time (Garcia-Anton, Cuezva, Fernandez-Cortes, Benavente, & Sanchez-Moral, 2014; Kuang, Jiao, & Li, 2013; Smith et al., 2003), leading to modulations of gas fluxes at the soil–atmosphere interface that must be understood. This is of particular importance when discrete flux measurements are integrated in space and/or time to quantify emissions or when flux measurements are used for detection, identification, or monitoring of a subsurface gas source. Many applications are related to greenhouse gases, such as the safety of CO_2 sequestration (Oldenburg, Mukhopadhyay, & Cihan, 2016),

Abbreviations: CEREEP, Centre de Recherche en Écologie Expérimentale et Prédictive; HDPE, high-density polyethylene; ROI, region of interest.

quantification of volcanic emissions (Camarda, Prano, Cappuzzo, Gurrieri, & Valenza, 2017), and C release from permafrost thaw (Schuur et al., 2015). Other applications are related to volatile contaminant plumes (natural attenuation or vapor extraction monitoring; Khan, Husain, & Hejazi, 2004), gas release in relation to hydraulic fracturing and shale gas production (Norris, Turcotte, Moores, Brodsky, & Rundle, 2016), and emissions of potentially toxic methylated trace elements from soils (Vriens, Lenz, Charlet, Berg, & Winkel, 2014). A third category of applications with growing importance is the detection of underground nuclear explosions in the framework of the Comprehensive Nuclear-Test-Ban Treaty (Carrigan & Sun, 2014; Carrigan, Sun, & Simpson, 2019).

Due to the complexity and high variability of gas-emitting natural systems, a reductionist approach is needed to decipher and quantify all processes influencing gas fluxes between soil and atmosphere. It would help in better constraining process-based models and achieving more accurate measurements and interpretations in field conditions. This has already been proposed by several groups that conducted column experiments. Small-size columns (1- to 10-cm scale) proved to be particularly relevant to study CO_2 respiration (Guo, Nishimura, Imoto, & Sun, 2015; Midwood, Thornton, & Millard, 2008). Decimeter- to meter-scale columns allow achieving experimental conditions closer to field conditions. Evans et al. (2001) assessed, using a dry sand column, the performance of accumulation chambers for volcanic or metamorphic CO_2 fluxes much higher than normally encountered in soil respiration studies. With simple laboratory sand column experiments, Ding, Kennedy, Evans, and Stonestrom (2016) and Sathaye, Larson, and Hesse (2016) evaluated the fractionation of noble gases as a tool to quantify gas dynamics in unsaturated porous media. These attempts used simplified abiotic systems and constant parameters. Some complexity of the natural systems was addressed using heterogeneous porous media (Ding, Kennedy, Molins, Kneafsey, & Evans, 2017; Plampin, Illangasekare, Sakaki, & Pawar, 2014), various soil textures with variable water content (Yang, Fan, & Jones, 2018), or sandstone cores (Kilgallon et al., 2018). However, there have been no experimental studies permitting evaluation of the coupling of physical, chemical, and biological processes on gas fluxes in soils. The purpose of the present study is to fill this gap using an innovative experimental setup that allows long-term and high-resolution gas flux measurements on an instrumented unsaturated meter-scale soil column under controlled yet variable environmental conditions in a climatic chamber. This setup was tested for different injection conditions of SF_6 (inert tracer gas) at the base of an unsaturated sand column subjected to barometric pressure fluctuations, plant growth, photosynthesis, respiration, lighting cycles, and watering. Another column without plants but subjected to the same tracer injections was simultaneously studied for comparison. The SF_6 and CO_2 fluxes at the soil surface were monitored with a 1-h time resolution during several months. While constant-mass flowrate injections were applied at the base of the columns, gas fluxes at the soil surface were shown to be controlled and modulated by processes of physical (pressure gradient, porosity), chemical (gas solubility), and biological (evapotranspiration, respiration) origins that are individually identified and discussed.

Core Ideas

- We performed a tracer gas percolation in unsaturated soil columns with plants.
- We used a long-term and high-resolution monitoring under controlled conditions.
- We show that gas fluxes depend on physical, chemical, and biological processes.
- Daytime modulations on gas fluxes are due to evapotranspiration from photosynthesis.
- Nighttime modulations on gas fluxes are due to plant-root respiration.

2 | MATERIALS AND METHODS

The experimental setup consisted of an instrumented vertical column filled with porous media completed by a gas injection unit at its base and a flux measurement device at its top. This experiment was performed in a climatic chamber. Setup and methods are presented below.

2.1 | Instrumented unsaturated column

A high-density polyethylene (HDPE) pipe of 36.5-cm i.d. (hence ~0.1 m^2 of surface area) formed a column containing the porous medium under investigation. The height of the column was adjusted to fit the water retention curve of the medium. In our application (see case study below), the column had a total length of 70 cm (Figure 1). A bottom plate with a central hole equipped with a stopcock was bolted to a flange at the base of the column. Above the bottom plate, a perforated polyvinyl chloride (PVC) annular mount supports a stainless-steel grid. This constituted a 12-cm-high gas injection unit (~12 L). A stainless-steel mesh filter sandwiched between two geotextiles rested on the grid and prevented the porous medium from falling into the injection unit. This defined the base of a 58-cm-high column (~60.7 L) to be filled with porous media. Ports equipped with air- and water-tight bulkhead connectors were installed along the column, allowing

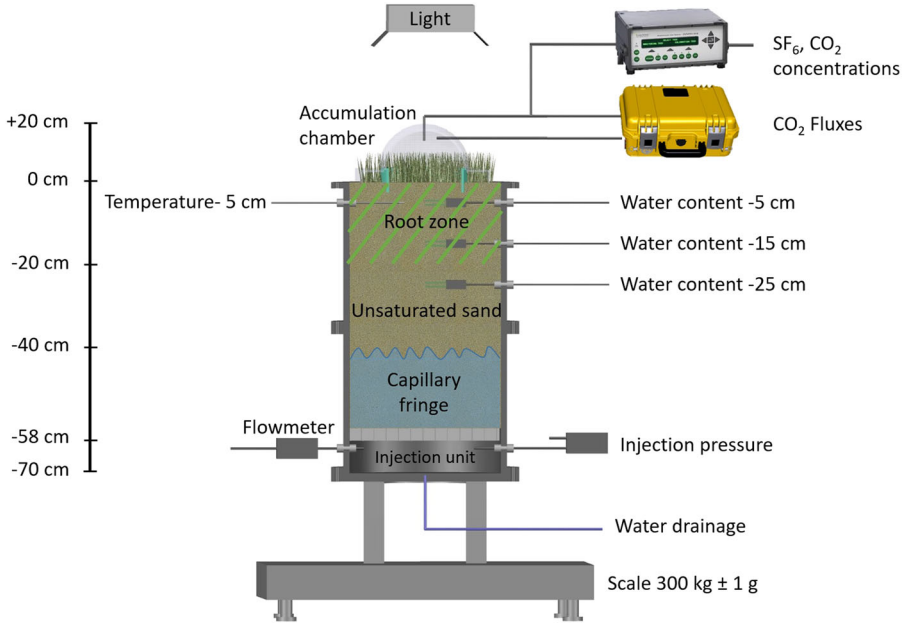

FIGURE 1 Cross-section of the experimental setup. From bottom to top: scale for water mass monitoring, column holder with water drainage system, chamber for tracer gas injection, porous membrane with membrane holder, unsaturated sand column (here shown with plants and with estimated root zone and capillary fringe), accumulation chamber in place for flux measurement with on-line gas monitoring by two gas analyzers (upper: LumaSense Innova 1412i, lower: LI-COR 8104C), a lighting system, and all additional sensors. The diameter of the column is 0.365 m with a surface area of 0.105 m^2. The diameter of the accumulation chamber is 0.203 m with a surface area of 0.0317 m^2

insertion of probes for various measurements or for tubing for obtaining gas and water samples. Gas and water sampling were not performed for this particular experiment. One port (at 5-cm depth) was used for inserting a temperature sensor (Pyrocontrol, PT100). The entire system was then pressure tested and found to be air tight. As shown in Figure 1, surface gas flux measurements were performed with an automated accumulation chamber on line with an infrared CO_2 analyzer (LI-COR 8104C) and a photo-acoustic field multi-gas analyzer (LumaSense, Innova 1412i) equipped for the determination of SF_6 and CO_2 concentrations. Details are given in the supplemental material.

The volumetric water content of the unsaturated porous medium in the column was monitored by means of probes measuring the dielectric constant of the soil (Decagon, MAS-1) inserted laterally at three different depths (5, 15, and 25 cm). In order to minimize adverse effects on gas and water flow in the column, the number of insertions and the size of the probes were restricted. Therefore, we did not monitor the capillary pressure and used the water retention curve determined in the laboratory for the studied porous medium. In addition, the total water budget was monitored by setting the instrumented column on a scale (Sartorius, Combics 1) with a capacity of 300 kg and an accuracy of 10^{-3} kg, which corresponds to better than 0.01 mm of water precipitation or evaporation.

All the sensors acquired data with a 5-min time resolution. We developed an acquisition system for all the instruments used in this experiment, based on Python, which recorded all parameters and measurements on the same terminal with a common time base, instead of using the various commercial software provided with the instruments with their time-stepping limitations. Signals from sensors (0–5 V or 4–20 mA) were collected by a Pyrocontrole PDM 8AI data logger linked to a computer.

2.2 | Gas injection design

A mixture of gases containing 10,000 µl L^{-1} of SF_6, with 20.9% O_2 and balanced in N_2, was injected at the base of the column through the injection unit. For advection–dispersion tests, tracer gas injections occurred at constant flow rate. A thermal mass flow regulator (Brooks Instruments, SLA 5850) was set to the target value, and the pressure in the injection unit was monitored. The differential pressure between the injection unit and the atmosphere was measured using a SETRA 267 pressure transducer, with a sensitivity of 2 Pa. Pressures and flowrates were recorded with accuracies better than 1%. For tracer tests performed in the diffusion regime instead of advection, the pressure in the injection unit was maintained equal to the ambient barometric pressure by opening one port to the atmosphere while injection of tracer gas in the chamber still occurred at 10 ml min^{-1}. In this manner, the tracer concentration applied at the bottom of the sand columns was kept constant without any pressure gradient, insuring diffusive conditions.

2.3 | Climatic chamber and experimental conditions

In order to better describe the influence of plants, an experiment using a column with plants (hereafter referred to as the plant column) and a control experiment using a column without plants (hereafter referred to as the control column) were run simultaneously. The complete setup is shown in Supplemental Figure S1.

The two columns were placed in a 13-m^3 climatic chamber (Ecolab) at the Centre de Recherche en Écologie Expérimentale et Prédictive (CEREEP)-Ecotron IleDeFrance center. Details and some applications of the Ecolab are given in Verdier et al. (2014). The ambient pressure in the climatic chamber was that of the atmosphere. Pressure and temperature inside the climatic chamber and outside were monitored with a Baro-Diver (Schlumberger Water Service) with a 5-min time resolution.

2.4 | Configuration of the studied case and material properties

Although the section above presented the general setup, the particular configuration of the studied case is detailed here. Two HDPE columns were filled with a homogeneous Fontainebleau sand (Sibelco NE 03) with a silica content larger than 99.88% (w/w) and a median grain size (D_{50}) of 213 μm. Each column was filled up to the top with successive 8- to 10-cm-thick layers of dry sand compacted by sedimentation in water, using a volume of water twice the volume of sand in the column. The volume of water then increased proportionally with the filling of the column. Each addition of a sand layer was followed by a draining period until almost no flow was observed at the bottom of the column; then, the same volume of water was added again twice. In this manner, we obtained a well-packed unsaturated sand column. The water retention curve of the studied sand was obtained from a combination of several laboratory measurements made at Institut National de la Recherche Agronomique (INRA) Avignon (France). From this, the capillary fringe of such a sand column was anticipated to rise up to ∼20 cm (i.e., 38 cm below the free surface). The intrinsic permeability of the sand column was estimated to be 3.6×10^{-12} m^{-2}.

In order to determine the maximum gas porosity of such sand columns, we used a column only filled with dry sand, using vibrations and compaction provided by handheld tools instead of sedimentation in water. The total porosity of such a dry sand column was determined to be 0.38 from its total volume and mass, knowing the density of silica (2.65 g cm^{-3}). This porosity was in agreement with results found in the laboratory.

In order to control and monitor environmental conditions, the experiment was performed in a climatic chamber at the CEREEP-Ecotron IleDeFrance. The ambient temperature inside the climatic chamber in this study was regulated at 25 °C. Temperature at the top at the column varied between 25 and 26 °C (depending if lighting was switched on or off). This was in good agreement with the target temperature, which was independent of the external temperature that varied between −12 and +20 °C. Drops of temperature at 5-cm depth were observed after watering events with colder tap water. The ambient pressure inside the climatic chamber was equal to the outside barometric pressure and followed natural variations between 980 and 1,030 mbar during the course of the experiment.

Artificial diurnal lighting was set for 12 h of daytime and 12 h of nighttime. To avoid accumulation of SF_6 in the climatic-chamber atmosphere, ambient air was renewed with a time constant of 0.07 s^{-1}. There was no moisture regulation in the chamber atmosphere and no wind. During the experiment, the two columns were kept under drying conditions. In order to maintain their initial water saturation profile, each column was manually and homogenously watered from the top with the same amount of water using a 60-ml syringe. Usual watering amounted to 1,800 ml, whereas some larger watering events reached 6,000 ml.

The tracer test was carried out using SF_6, an inert tracer gas commonly used that has a very low natural abundance in the atmosphere. A mixture of N_2 (balance), O_2 (20%), and SF_6 (10,000 μl L^{-1}) was injected at the base of the columns with various constant flowrates from 10 to 100 ml min^{-1} in normal conditions (0 °C and 101,325 Pa), as detailed in Table 1. From these values, one can calculate the theoretical flux applied at the base of each column and expected at the surface after a steady state is achieved.

Three weeks before gas injection, the plant column was densely seeded at its top with 8 g of fescue (*Festuca arundinacea* Schreb.) seeds, a perennial grass. The seeds were covered by 3 cm of sand and gently compacted by hand, then watered. More than half of the seeds finally germinated. At the time of tracer injection, the plants already reached a significant size (∼5 cm). After a growth period of 12 wk, we cut the grass shoots at 2 cm above ground level. Then, we let the plants grow again.

3 | RESULTS

3.1 | Plant growth

During the experiment, the blades of grass (for the plant column) reached a maximum height of 15 cm, before being cut on Day 39, 78 d after seeding. As shown by post-experiment examination (see Supplemental Figure S2), the root zone

TABLE 1 Tracer injection conditions observed SF_6 fluxes and plant status

Parameter	Time					
	0–1 d	1–6 d	6–12 d	12–21 d	21–54 d	54–61 d
SF_6, µl L^{-1}	10,000	10,000	10,000	10,000	10,000	10,000
Flowrate, ml min^{-1}	100	50	20	10	10	10
Percolation regime[a]	AD	AD	AD	AD	D	AD
Integrated imposed flux[b], mmol	65	202	69	50	NS[c]	40
Integrated/observed flux[d], mmol	42/37	163/149	58/52	43/46	NS	31/35
Observed/imposed, %	65/56	81/74	83/75	85/91	NS	77/86
Plant status	Growth	Growth	Growth	Growth	Cut on Day 39	Growth

[a]AD, advection–dispersion; D, diffusion only.

[b]By advection only.

[c]NS, not significant.

[d]At the surface of the plant and the control columns, respectively.

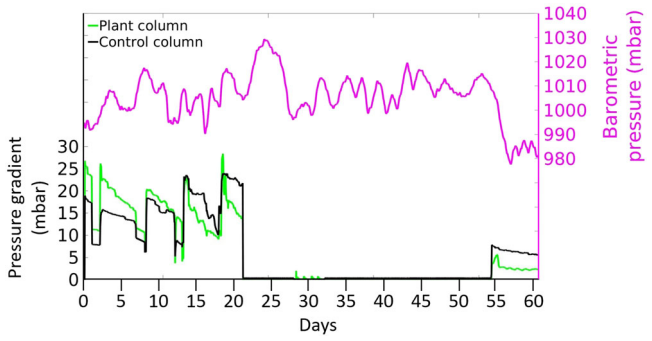

FIGURE 2 Pressure conditions as a function of time (5-min time resolution) during tracer experiments with various injection characteristics as detailed in Table 1, for the plant and the control columns. The pressure gradient is the difference between the pressure in the injection unit at the base of the column and the barometric pressure over a length of 58 cm corresponding to the height of the column. Opening of the injection unit occurred on Days 0, 2, 6–7, 12, 21, and 28

reached a minimum depth of 18 cm, with a dense zone of ~6 cm, a moderately dense zone of ~6 cm, and a sparse zone of ~6 cm or more.

3.2 | Results from long-term and high-resolution monitoring

In this section, we present the pressure conditions, the water budget, and the gas fluxes monitored over a period of 61 d during the tracer experiment.

3.2.1 | Injection pressure

As shown in Figure 2, the pressure of the tracer gas in the injection unit varied between 0 and +30 mbar relative to the barometric pressure, in response to the various targeted flowrates (Table 1). During injection, sudden pressure drops corresponded to the brief opening of the injection unit to the atmosphere in order to take action on the setup for maintenance (Days 2, 6–7, and 12), to drain out water accumulated due to natural drainage of the soil column (Day 28) or to switch the injection from advection to diffusion (Day 21). During the tracer test in diffusion conditions, pressure in the injection unit was kept equal to that of the atmosphere by opening the chamber to the atmosphere. However, some minor pressure changes could be observed between Days 28 and 32.

3.2.2 | Time and space evolution of water content in the sand columns

The time evolution of the water budget was precisely quantified by monitoring the total mass variations of each column (Figure 3). The water content is expressed relative to the equilibrium water content originally obtained after natural draining of the saturated sand columns shortly after completion. The gain in mass was not corrected for biomass production in the plant column, which remained minor (<0.5%). Three types of water content evolution can be observed: sharp increases, progressive decreases, and sharp decreases. Ordinary watering events lead to sharp mass increases of ~1,800 g, whereas a large watering event lead to sharp mass increases of ~6,000 g. Watering occurred every 5–7 d in the first half of the experiment, then was switched to everyday, while occurring once in 25 d at the end. Sharp mass decreases correspond to water being drained out from the injection unit, whereas progressive mass decreases correspond to evaporation. The evaporation rate is larger in the plant column than in the control column. Periodic changes in the evaporation rate are observed in the plant column (inset Figure 3), and they correspond to the imposed daytime–nighttime cycle. During nighttime, the evaporation rate in the plant column is similar to the one in the control column, whereas it is two times larger during daytime.

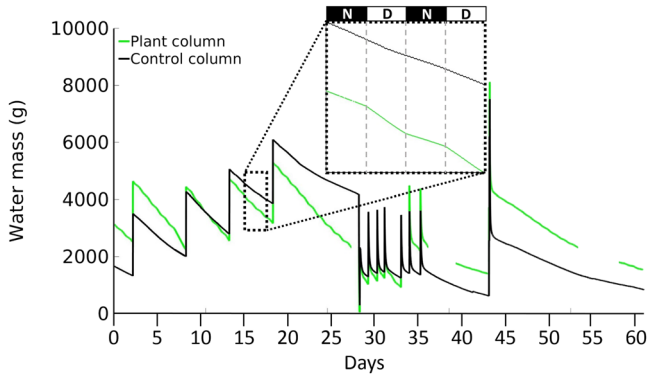

FIGURE 3 Fluctuations of the mass of water with a 5-min time resolution for the plant column (green) and the control column (black). The water mass is expressed as excess compared with the original equilibrium water content. Sharp increases in mass are due to watering; sharp decreases are due to water being drained out of the injection unit; progressive mass decreases are due to physical evaporation alone in the control column and the combination of physical evaporation (during nighttime [N]) and biologically driven evaporation (transpiration, during daytime [D]) in the plant column (see inset)

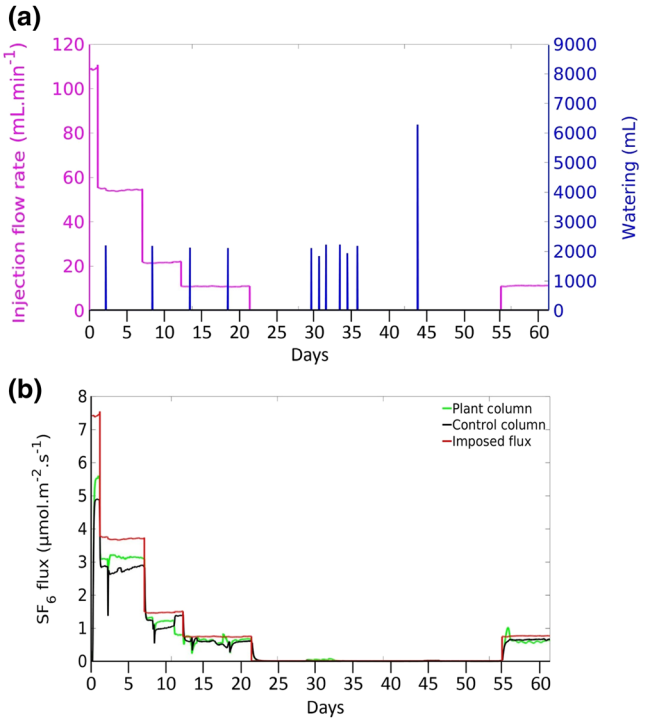

FIGURE 4 SF_6 percolation during the total period of the experimental study in the plant and control columns. (a) Injection flowrate (pink) as a function of time and amount of water used for each watering event (blue). Between Days 21 and 54, tracer test was conducted under diffusion conditions. (b) The SF_6 fluxes observed at the surface of the plant (green) and control (black) columns in response to tracer injection over a period of 61 d with a 1-h time resolution. The tracer flux applied at the base of the columns is reported in red. Differences between imposed and observed fluxes are discussed in the text

3.2.3 | Tracer fluxes at the top of the columns

The SF_6 fluxes measured at the top of the plant and control columns in response to the tracer injections are presented in Figure 4b. Applied flow rates and watering events are represented in Figure 4a. The observed surface fluxes are also reported in Table 1, for further comparison with the applied fluxes. As expected, the SF_6 fluxes looked similar for both columns and increased when the flowrate applied at the base of a given column and/or the concentration of the tracer increased. During the diffusion period (Days 21–54), no flux could be detected at the surface of both columns, the calculated flux being not significantly different from the situation before any tracer injection. An exception was between Days 28 and 32, where some minor fluxes could be measured (<0.04 µmol m^{-2} s^{-1}). Variations in injection pressure could also be observed at this period. Watering events were associated with transient and sharp decreases in SF_6 surface fluxes.

4 | DISCUSSION

While injections at constant flowrate were applied at the base of the columns, gas fluxes at the soil surface appeared to be controlled and modulated by processes that are individually identified and discussed below. These processes are of several origins: physical (pressure gradient, porosity), chemical (gas solubility), and biological (evapotranspiration, respiration).

4.1 | Variations of the water budget: Planted vs. bare soil

The very sensitive monitoring of the water mass (corresponding to 0.01 mm or 1 ml for each column, Figure 3) allowed us to observe the control of plant activity on the water budget, although the biome considered here was quite modest. As determined from Figure 3, the evaporation rate for the control column subjected to physical evaporation alone was ~1 L m^{-2} every 12 h. In the plant column during nighttime, physical evaporation alone also occurred at ~1 L m^{-2} every 12 h. However, during daytime in the plant column, biologically driven evaporation (transpiration) was ~2 L m^{-2} every 12 h, Thus, modulations of water loss with a 12-h period controlled by lighting are observed in the plant column. By contrast, with natural conditions, physical evaporation occurred at the same rate during daytime and nighttime in the experiment for both columns because the conditions in the climatic chamber (including temperature and humidity) were kept constant. During the tracer experiment, the evaporation rate in the

control column tended to decrease, from ~1 to 0.6 L m^{-2} every 12 h . This goes with an overall decreasing amount of water in the column (Figures 3). The evaporation rate in the plant column was also decreasing after Day 39, which was due to the plant having been cut.

Plant and control columns reacted differently to events such as watering, infiltration, drainage, and evaporation. In fact, the plant column drained more easily than the control column, which is explained by the vertical anisotropy due to plant roots. Furthermore, during watering, infiltration was observed to be slower in the control column, which developed a very fine layer with low permeability at its surface. Neave and Rayburg (2007) and Armenise et al. (2018) reported that water drops and surficial evaporation can locally compact sand, creating a fine crust of low permeability, limiting infiltration at depth. Evaporation of this surface water causes less water to be transferred to the bottom of the control column, as reported in Supplemental Figure S3.

During Days 21–54, tracer injection in diffusion conditions stopped the overpressure (≤30 mbar) in the injection unit. This resulted in an immediate loss of water in both columns. These losses of water in both columns are interpreted as drainage being increased at the base of the columns when the pressure applied at the bottom ceased and less water could be held back.

4.2 | Comparison between injected and measured sulfur hexafluoride fluxes

As reported in Table 1 and Figure 4, the SF_6 fluxes measured at the surface of the columns are lower than or equal to the applied ones. For each injection period, the observed surface flux globally paralleled the applied one and accounted for 80–90% of the applied flux (Table 1), except during the first day when a steady state was probably not reached. Part of the 10–20% discrepancy between the observed and the applied fluxes could be explained by the uncertainty in the flux measurement. However, this discrepancy is not likely to be caused by a bias in the flux determination (no wind, constant temperature and humidity, similar CO_2 flux determination with the automated Li-COR method and with our own method). We favor a cause linked to gas percolation in the unsaturated sand columns. As detailed in the supplemental material, SF_6 solubility in water cannot account for a significant loss of tracer. The accumulation chambers used for flux determination only covered 30% of the surface area of the columns and could not be moved from the center of the columns. Heterogeneity in the surface flux due to preferential flow is likely. Preferential pathways or channeling is a common process in porous media, especially when a gas phase is forced to infiltrate into a saturated zone (Islam, Chevalier, Salem, & Sassi, 2018; Kong, Kinzelbach, & Stauffer, 2010).

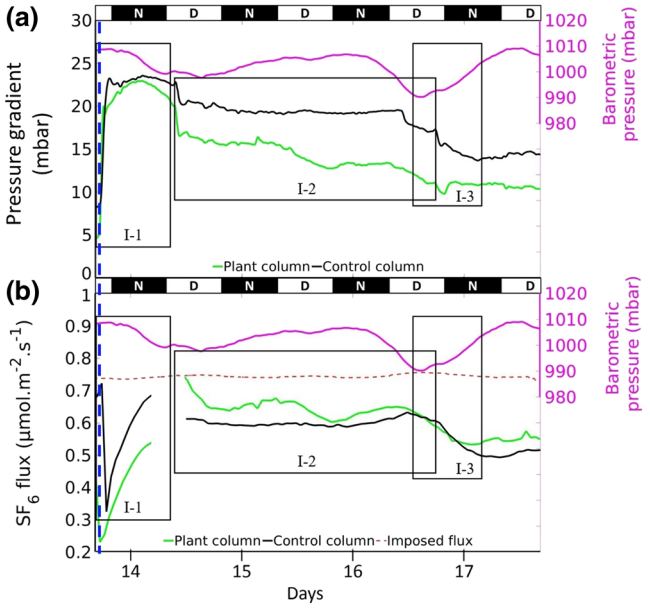

FIGURE 5 Relationship between pressure fluctuations and surface gas fluxes shown on an expanded timescale between the 14th and the 17th day of the experiment. (a) Variations of the pressure gradient between the bottom and the top of the column over a distance of 58 cm and (b) variations in the measured SF_6 surface fluxes as a function of time during a constant-flowrate injection at the bottom of the plant and of the control columns. Daytime (D) and nighttime (N) 12-h cycles are indicated. The red dashed line corresponds to the applied flux at the base of the columns. The blue dashed line corresponds to watering. The three regions of interest depicted by rectangles and labeled are discussed in the text

4.3 | Pressure control on sulfur hexafluoride surface fluxes and additional influences

To study how the SF_6 surface fluxes are related to external forcing, we here focus on two limited periods of time between Days 13–18 (Focus I) and Days 54–61 (Focus II). The corresponding variations in the difference between injection pressure and the barometric pressure are reported in Figures 5a and 6a, respectively, whereas the barometric pressure and SF_6 fluxes are reported in Figures 5b and 6b. As the height of the column is constant, the difference between the injection pressure and the barometric pressure directly relates to the pressure gradient, which is an important control on advection, together with the relative gas permeability. Three regions of interest (ROIs) can be delimited in Focus I (ROIs I-1–I-3, Figure 5), and two can be delimited in Focus II (ROIs II-1 and II-2, Figure 6).

As shown in ROI I-1, watering was responsible for a rapid pressure increase in the pressure gradient in both columns (Figures 5a), first associated with a ~50% decrease in the SF_6 fluxes (Figure 5b), followed by a significant increase in the SF_6 fluxes. Water infiltration strongly decreases gas

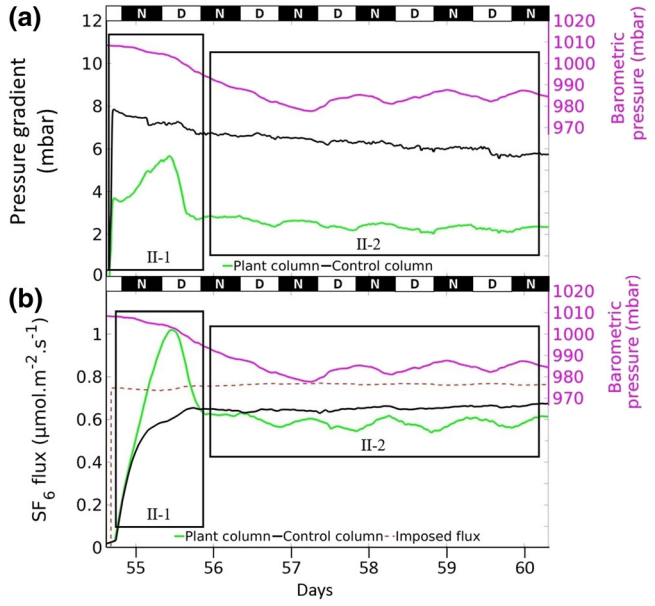

FIGURE 6 Relationship between pressure fluctuations and surface gas fluxes shown on an expanded timescale for the 55th through 60th day of the study. (a) Variations of the pressure gradient between the bottom and the top of the column over a distance of 58 cm and (b) variations in the measured SF_6 surface fluxes as a function of time during a constant-flowrate injection at the bottom of the plant and of the control columns. Daytime (D) and nighttime (N) 12-h cycles are indicated. The red dashed line corresponds to the applied flux at the base of the columns. The blue dashed line corresponds to the watering. The two regions of interest depicted by rectangles and labeled are discussed in the text

porosity and thus the relative gas permeability, which in turn decreases the SF_6 flux, leading to a transient overpressure in the injection unit and ultimately leading to preferential flow with a transient high SF_6 flux. These events illustrate that gas injected in the injection unit must push back water from the capillary fringe in order to percolate in the unsaturated sand columns, most probably forming preferential flow by fingering, as shown by Kong et al. (2010) and Islam et al. (2018).

A similar effect of overpressure on the SF_6 flux was observed (ROI II-1, Figure 6a). This time, overpressure did not come from water infiltration but from injection conditions being turned from diffusion to advection on Day 54. Again, the rapid increase in pressure was followed by a more progressive increase in SF_6 flux. The nearly constant pressure gradient over >4 d is then associated with a nearly constant SF_6 flux. Only a transient increase in pressure gradient in the plant column on Day 55 resulted in a transient enhanced flux.

The overall decrease in pressure gradient shown in Figure 5a, particularly for the plant column, corresponds with drying conditions lasting several days (see Figure 3). Less water in the column allows for more gas to flow in at lower pressure from the injection unit. Correlatively, SF_6 fluxes decreased (Figure 5b). The decrease in SF_6 flux was larger in the plant column than in the control column, with the decrease in pressure gradient being larger for the plant column than for the control column, and the evapotranspiration rate in the plant column being larger than the rate of physical evaporation alone in the control column.

In ROI I-2 (Figure 5b) and ROI II-2 (Figure 6b), SF_6 fluxes in the plant column show daily ups and downs, whereas SF_6 fluxes in the control column appear monotonous. Although barometric pressure might also show some variations of the same kind, particularly during Days 57–60 in ROI II-2, there is no correlation between SF_6 flux and barometric pressure (as also shown in Figure 5b), and it is expected that the control column would behave the same as the plant column. Thus, we favor another forcing, different from a pressure effect and related to the plants that will be studied in more detail in a separate section below.

As shown in ROI I-3 of Figure 5a, the pressure gradients for the plant and the control columns decreased similarly when barometric pressure started to increase by +20 mbar in the middle of Day 16. Because it was applied externally, this forcing was the same for both columns and resulted in similar decreases in SF_6 fluxes.

4.4 | Biological controls on diurnal variations of the sulfur hexafluoride flux for the plant column

As highlighted in ROIs I-2 (Figure 5b) and II-2 (Figure 6b), SF_6 fluxes in the plant column globally show daily ups and downs, whereas SF_6 fluxes in the control column appear monotonous. In order to understand if biological activity could be the factor controlling such fluctuations in the SF_6 flux, the SF_6 and CO_2 fluxes measured at the surface of the plant column are reported in Figure 7a for Focus I and Figure 8a for Focus II, with indications of daytime and nighttime. For the same periods, the time evolution of the water mass in the plant column and of the pressure gradient are reported in Figures 7b and 8b.

During daytime, the net measured surface CO_2 fluxes are negative, indicative as expected of photosynthesis, and the SF_6 fluxes are shown to decrease systematically (Figures 7a and 8a). During photosynthesis, CO_2 and H_2O are consumed and combined in plants to produce organic matter and O_2. At the same time, an elevated rate of water loss by evapotranspiration is observed together with a decrease in the pressure gradient in the plant column (Figures 7b and 8b). This is interpreted as being due to an increase in gas porosity and relative air permeability. This leads to more dispersion and storage of gases in the porous medium and explains the observed transient decrease in SF_6 flux although the applied SF_6 flowrate at the base of the column was constant.

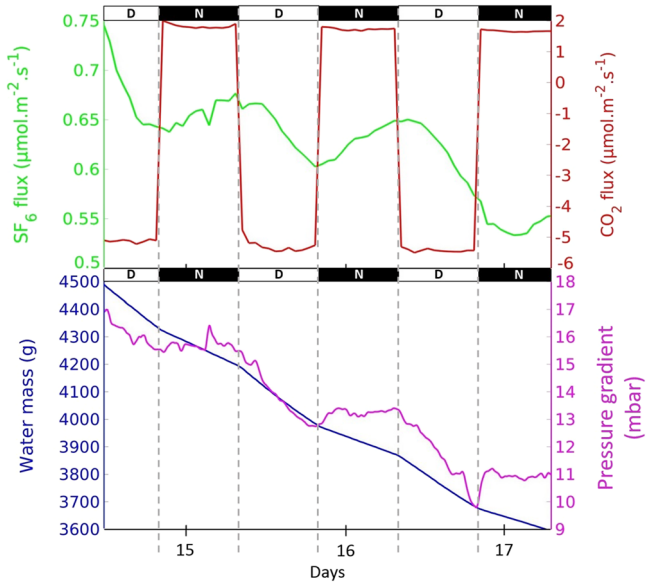

FIGURE 7 Modulations of the SF_6 surface flux by plant activity during a period of 3 d. (a) Time evolution of the SF_6 and CO_2 fluxes; (b) time evolution of the water mass and pressure gradient between the bottom and the top of the column over a distance of 58 cm. Daytime (D) and nighttime (N) 12-h cycles are indicated. The time variations of the water mass and the pressure gradient are correlated only during daytime, when photosynthesis and evapotranspiration are active. This enhanced loss of water increases gas porosity, which periodically decreases the pressure gradient

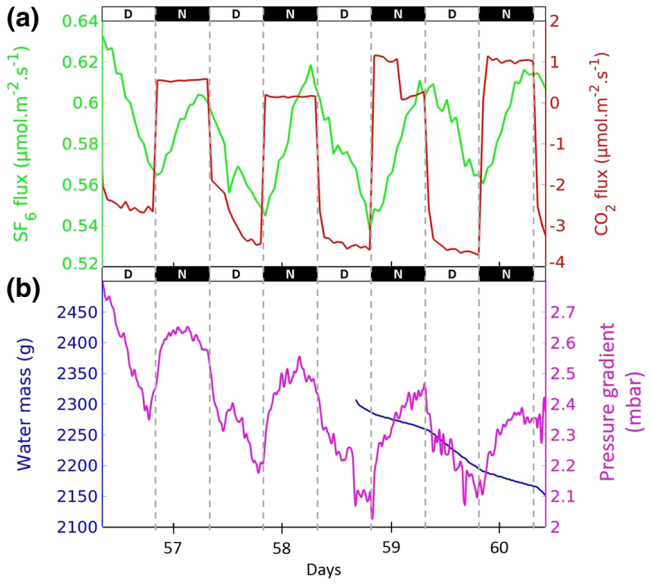

FIGURE 8 Modulations of the SF_6 surface flux by plant activity during a period of 4 d. (a) Time evolution of the SF_6 and CO_2 fluxes; (b) time evolution of the water mass and pressure gradient between the bottom and the top of the column over a distance of 58 cm. Daytime (D) and nighttime (N) 12-h cycles are indicated

During nighttime, the observed surface CO_2 fluxes are positive, indicative (as expected) of plant respiration only, and the SF_6 fluxes are shown to increase systematically (Figures 7a and 8a). Plant respiration in the root zone consumes organic matter and O_2 to produce CO_2 and H_2O. At the same time, a moderate water loss due to physical evaporation alone is observed (Figures 7b and 8b), whereas the pressure gradient shows a minor increase then stays relatively constant, particularly in Focus I (Figure 7b). The much smaller range of pressure fluctuations during Focus II (0.8 mbar in 3 d) compared with Focus I (8 mbar in 3 d) allows a better illustration of the evolution of the pressure gradient during nighttime. The fluctuations, with an amplitude of 0.3–0.4 mbar, appear to have reproducible characteristic shapes consisting of an increasing exponential function followed by a decreasing exponential function that continues over the following daytime period.

Despite these relatively small changes in pressure gradient between the bottom and the surface of the sand column and the constant applied SF_6 flowrate at the base of the column, a transient increase in SF_6 surface flux by 5–15% is observed. Because respiration in the root zone is always active (daytime and nighttime), CO_2 produced by respiration cannot be responsible for scavenging of SF_6, which should only be active at night to explain why SF_6 fluxes are only enhanced during nighttime. Therefore, this mechanism cannot account for an enhanced SF_6 flux only during nighttime. We favor a mechanism linked to the CO_2 production and O_2 consumption during nighttime, inspired by the work of Freundt, Schneider, and Aeschbach-Hertig (2013) and Guillon, Gréau, and Pili (2016), done in another context. Carbon dioxide produced by respiration in the root zone has a solubility higher by one order of magnitude in pore water than the O_2 that it replaces (Sander, 2015). Larger dissolution of CO_2 relative to O_2 locally decreases the pore pressure and increases the pressure gradient between the base of the column and the root zone, although this is not observed by measuring the overall difference between the injection pressure in the injection unit and the barometric pressure. This enhanced pressure gradient increases transport of SF_6 towards the root zone (which is denser and thus more active within the first 6 cm below surface), from which SF_6 will easily be emitted to the atmosphere.

This biologically driven control on surface gas fluxes observed here for a very modest biome (see Supplemental Figure S2) accounted for ~10% of the variations of the flux. It could well be much higher for larger biomes, such as meadows or forests, because it scales with the intensity of evapotranspiration and root respiration (Bosquilia et al., 2019; Pauliukonis & Schneider, 2001). Also, microbiological activity known to be active in natural soils would enhance the respiration effect, whereas it is much more likely limited in our studied case of a model soil consisting of washed pure silica sand.

5 | CONCLUSIONS

We developed an innovative laboratory experiment dedicated to the long-term and high-resolution monitoring of gas fluxes of a planted unsaturated soil column placed under controlled conditions in a climatic chamber. This includes controlled tracer injections at constant flowrate at the bottom of the column and very sensitive water budget monitoring. A control column of the same soil without plants was subjected to the same conditions for reference. This setup features a validated approach that allows determination of surface fluxes of any gas of interest using commercially available accumulation chambers, originally dedicated to CO_2 fluxes and here coupled with any low-flow gas analyzers. This innovative setup was used to better understand the processes and parameters determining gas transport through porous media and surface gas fluxes at the laboratory scale, and particularly to disentangle the physical, chemical, and biological influences, as well as their interactions. This setup presents many opportunities for further applications and studies.

Several percolation experiments using SF_6 as a tracer gas were conducted with various flowrates at 10,000 µl L^{-1}. Tracer injection under diffusion conditions led to gas fluxes too small to be detected. When advection occurs, we found that the pressure gradient and the relative gas permeability were not the only factors influencing surface gas fluxes, and we highlighted a biological effect. Although constant fluxes were applied at the bottom of the columns, the surface SF_6 fluxes were highly dynamical with transient states in relation to the applied external forcing. The injection pressure applied at the bottom of each column and the barometric pressure at the surface determined the pressure gradient. The water content then controlled, at the same time, a pressure head (determining an air-entry pressure for the injection) and the relative gas permeability and porosity in the porous media. Water infiltration strongly decreases gas porosity and the relative gas permeability, which in turn decreases the tracer flux, leading to a transient overpressure at the base of the column and ultimately triggering or enhancing preferential flow, resulting in a transient high SF_6 flux. On a longer timescale, water content was controlled by transpiration during daytime in the planted soil column and by physical evaporation alone in the bare soil column, as well as during nighttime for the plant column. Increasing water loss not only increases the relative gas permeability or decreases the pressure gradient by decreasing the injection pressure, but also increases gas porosity, which in turn increases gas storage and decreases the surface gas flux.

Both high-resolution and high-sensitivity monitoring permitted observation of diurnal modulations of surface gas fluxes in the plant column interpreted as a biological influence. It here accounted for 5–15% of the flux variations and could account for much more in larger biomes such as forests or microbiologically active soils. This biologically driven influence is twofold: (a) plant evapotranspiration during daytime increases water loss, hence the porosity and the relative gas permeability, and (b) respiration by plant roots and microorganisms results in O_2 consumption and CO_2 production; the higher solubility of CO_2 in water locally diminishes pore pressure, increasing the pressure gradient towards the root zone, hence the tracer flux.

Therefore, physical, chemical, and biological processes altogether influence surface gas fluxes. Although the applied tracer gas flux was constant, these coupled processes accounted for transient decreases or increases of the observed surface fluxes on timescales spanning from several hours to several days. This has important consequences when discrete flux measurements are integrated in space and/or in time to quantify emissions or when used for detection and identification of underground gas sources. One-time gas collection can lead to erroneous estimates of fluxes due to high space and time variability. In addition, modulations of gas release to the atmosphere resulting from these processes should be taken into account for improved models of the time-dependent atmospheric signature of a gas source originating in the subsurface (Carrigan et al., 2019). Future modeling efforts with the NUFT (Nonisothermal, Unsaturated Flow, and Transport with Chemistry) code (Nitao, 1998) will seek to provide further refinement of quantification and prediction capabilities.

CONFLICT OF INTEREST

The authors declare that they have no known conflicting financial interests or personal relationships that could have appeared to influence the work reported in this paper.

AUTHOR CONTRIBUTIONS

All authors participated in the design of the experiment. C.A., E.P., F.M., and S.C. assembled and maintained the experimental device. C.A. ran the experiments and collected the data. C.A. and E.P. analyzed the data. C.A., E.P., and P.B. discussed the results. E.P., C.A., and P.B. wrote the manuscript.

ACKNOWLEDGMENTS

This study was carried out in the framework of the Laboratoire de Recherche Conventionné (LRC) Yves-Rocard joint laboratory between the Commissariat à l'énergie atomique (CEA) and École normale supérieure (ENS). This work also benefited from technical and human resources provided by the Centre national de la recherche scientifique (CNRS) Infrastructures de Recherche (IR) ECOTRONS and CEREEP-Ecotron IleDeFrance (CNRS/ENS UMS 3194), as well as financial support from the Regional Council of Ile-de-France under the DIM (Domains of Major Interest) Program R2DS bearing the reference I-05-098/R and 2011-11017735 and from the European Union Fonds Européens de Développement Régional (FEDER) program 2007–2014. It received support under the program "Investissements

d'Avenir" launched by the French government and implemented by the Agence nationale de la recherche (ANR) with the reference ANR-11-INBS-0001 AnaEE France and ANR-10-IDEX-0001-02-PSL. Amandine Hansart is thanked for assistance in choosing and growing plants and for advice for watering. Jean-François Le Galliard, Florent Barbecot, and Sophie Guillon are thanked for fruitful discussions. We thank two anonymous reviewers as well as Scott Jones as associate editor for their comments that greatly helped improve the manuscript.

ORCID

Clement Alibert https://orcid.org/0000-0002-8032-1140
Eric Pili https://orcid.org/0000-0002-5328-2107
Pierre Barre https://orcid.org/0000-0002-0822-0556
Florent Massol https://orcid.org/0000-0001-5017-121X
Simon Chollet https://orcid.org/0000-0001-7551-6616

REFERENCES

Armenise, E., Simmons, W. S., Ahn, A., Garbout, A., Doerr, S. H., Mooney, S. J., … Ritz, K. (2018). Soil seal development under simulated rainfall: Structural, physical and hydrological dynamics. *Journal of Hydrology*, *556*, 211–219. https://doi.org/10.1016/j.jhydrol.2017.10.073

Bosquilia, R. W. D., Neale, C. M. U., Duarte, S. N., Longhi, S. J., Ferraz, S. F., de, B., & Muller-Karger, F. E. (2019). Evaluation of evapotranspiration variations according to soil type using multivariate statistical analysis. *Geoderma*, *355*. https://doi.org/10.1016/j.geoderma.2019.113906

Camarda, M., Prano, V., Cappuzzo, S., Gurrieri, S., & Valenza, M. (2017). Temporal variations in air permeability and soil CO_2 flux in volcanic ash soils (island of Vulcano, Italy). *Geochemistry Geophysics Geosystems*, *18*, 3241–3253. https://doi.org/10.1002/2017GC006857

Carrigan, C. R., & Sun, Y. W. (2014). Detection of noble gas radionuclides from an underground nuclear explosion during a CTBT on-site inspection. *Pure and Applied Geophysics*, *171*, 717–734. https://doi.org/10.1007/s00024-012-0563-8

Carrigan, C. R., Sun, Y., & Simpson, M. D. (2019). The characteristic release of noble gases from an underground nuclear explosion. *Journal of Environmental Radioactivity*, *196*, 91–97. https://doi.org/10.1016/j.jenvrad.2018.10.015

Ding, X., Kennedy, B. M., Evans, W. C., & Stonestrom, D. A. (2016). Experimental studies and model analysis of noble gas fractionation in porous media. *Vadose Zone Journal*, *15*(2), vzj2015.06.0095. https://doi.org/10.2136/vzj2015.06.0095

Ding, X., Kennedy, B. M., Molins, S., Kneafsey, T., & Evans, W. C. (2017). Experimental studies and model analysis of noble gas fractionation in low-permeability porous media. *Geochimica et Cosmochimica Acta*, *205*, 149–167. https://doi.org/10.1016/j.gca.2017.02.005

Evans, W. C., Sorey, M. L., Kennedy, B. M., Stonestrom, D. A., Rogie, J. D., & Shuster, D. L. (2001). High CO_2 emissions through porous media: Transport mechanisms and implications for flux measurement and fractionation. *Chemical Geology*, *177*, 15–29. https://doi.org/10.1016/S0009-2541(00)00379-X

Freundt, F., Schneider, T., & Aeschbach-Hertig, W. (2013). Response of noble gas partial pressures in soil air to oxygen depletion. *Chemical Geology*, *339*, 283–290. https://doi.org/10.1016/j.chemgeo.2012.07.026

Garcia-Anton, E., Cuezva, S., Fernandez-Cortes, A., Benavente, D., & Sanchez-Moral, S. (2014). Main drivers of diffusive and advective processes of CO_2-gas exchange between a shallow vadose zone and the atmosphere. *International Journal of Greenhouse Gas Control*, *21*, 113–129. https://doi.org/10.1016/j.ijggc.2013.12.006

Guillon, S., Gréau, C., & Pili, E. (2016). Continuous monitoring of the vadose zone gas phase by mass spectrometry. *Vadose Zone Journal*, *15*(8), vzj2015.12.0168. https://doi.org/10.2136/vzj2015.12.0168

Guo, L. L., Nishimura, T., Imoto, H., & Sun, Z. G. (2015). Applicability of soil column incubation experiments to measure CO_2 efflux. *International Agrophysics*, *29*, 413–421. https://doi.org/10.1515/intag-2015-0047

Hutchinson, G. L., & Mosier, A. R. (1981). Improved soil cover method for field measurement of nitrous oxide fluxes. *Soil Science Society of America Journal*, *45*, 311–316. https://doi.org/10.2136/sssaj1981.03615995004500020017x

Islam, A., Chevalier, S., Salem, I. B., & Sassi, M. (2018). Numerical simulation of gas injection in vertical water saturated porous media. *Environmental Modeling and Assessment*, *23*, 459–469. https://doi.org/10.1007/s10666-017-9587-x

Khan, F. I., Husain, T., & Hejazi, R. (2004). An overview and analysis of site remediation technologies. *Journal of Environmental Management*, *71*, 95–122. https://doi.org/10.1016/j.jenvman.2004.02.003

Kilgallon, R., Gilfillan, S. M. V., Edlmann, K., McDermott, C. I., Naylor, M., & Haszeldine, R. S. (2018). Experimental determination of noble gases and SF_6, as tracers of CO_2 flow through porous sandstone. *Chemical Geology*, *480*, 93–104. https://doi.org/10.1016/j.chemgeo.2017.09.022

Kong, X-Z., Kinzelbach, W., & Stauffer, F. (2010). Morphodynamics during air injection into water-saturated movable spherical granulates. *Chemical Engineering Science*, *65*, 4652–4660. https://doi.org/10.1016/j.ces.2010.05.007

Kuang, X. X., Jiao, J. J., & Li, H. L. (2013). Review on airflow in unsaturated zones induced by natural forcings. *Water Resources Research*, *10*, 6137–6165. https://doi.org/10.1002/wrcr.20416

Midwood, A. J., Thornton, B., & Millard, P. (2008). Measuring the ^{13}C content of soil-respired CO_2 using a novel open chamber system. *Rapid Communications in Mass Spectrometry*, *22*, 2073–2081. https://doi.org/10.1002/rcm.3588

Neave, M., & Rayburg, S. (2007). A field investigation into the effects of progressive rainfall-induced soil seal and crust development on runoff and erosion rates: The impact of surface cover. *Geomorphology*, *87*, 378–390. https://doi.org/10.1016/j.geomorph.2006.10.007

Nitao, J. J. (1998). *User's manual for the USNT module of the NUFT code, Version 3.0 (NP-phase, NC-Component, Thermal)*. Livermore, CA: Lawrence Livermore National Laboratory.

Norris, J. Q., Turcotte, D. L., Moores, E. M., Brodsky, E. E., & Rundle, J. B. (2016). Fracking in tight shales: What is it, what does it accomplish, what are its consequences? *Annual Review of Earth and Planetary Sciences*, *44*, 321–351. https://doi.org/10.1146/annurev-earth-060115-012537

Oldenburg, C. M., Mukhopadhyay, S., & Cihan, A. (2016). On the use of Darcy's law and invasion-percolation approaches for modeling large-scale geologic carbon sequestration. *Greenhouse Gases: Science and Technology*, *6*, 19–33. https://doi.org/10.1002/ghg.1564

Pauliukonis, N., & Schneider, R. (2001). Temporal patterns in evapotranspiration from lysimeters with three common wetland plant species in the eastern United States. *Aquatic Botany*, *71*, 35–46. https://doi.org/10.1016/S0304-3770(01)00168-1

Plampin, M., Illangasekare, T., Sakaki, T., & Pawar, R. (2014). Experimental study of gas evolution in heterogeneous shallow subsurface formations during leakage of stored CO_2. *International Journal of Greenhouse Gas Control*, *22*, 47–62. https://doi.org/10.1016/j.ijggc.2013.12.020

Sander, R. (2015). Compilation of Henry's law constants for water as solvent. *Atmospheric Chemistry and Physics*, *15*, 4399–4981. https://doi.org/10.5194/acp-15-4399-2015

Sathaye, K. J., Larson, T. E., & Hesse, M. A. (2016). Noble gas fractionation during subsurface gas migration. *Earth and Planetary Science Letters*, *450*, 1–9. https://doi.org/10.1016/j.epsl.2016.05.034

Schuur, E. A. G., McGuire, A. D., Schadel, C., Grosse, G., Harden, J. W., Hayes, D. J., … Vonk, J. E. (2015). Climate change and the permafrost carbon feedback. *Nature*, *520*, 171–179. https://doi.org/10.1038/nature14338

Smith, K. A., Ball, T., Conen, F., Dobbie, K. E., Massheder, J., & Rey, A. (2003). Exchange of greenhouse gases between soil and atmosphere: Interactions of soil physical factors and biological processes. *European Journal of Soil Science*, *54*, 779–791. https://doi.org/10.1046/j.1351-0754.2003.0567.x

Verdier, B., Jouanneau, I., Simonnet, B., Rabin, C., Van Dooren, T. J. M., Delpierre, N., … Le Galliard, J. F. (2014). Climate and atmosphere simulator for experiments on ecological systems in changing environments. *Environmental Science and Technology*, *48*, 8744–8753. https://doi.org/10.1021/es405467s

Vriens, B., Lenz, M., Charlet, L., Berg, M., & Winkel, L. H. E. (2014). Natural wetland emissions of methylated trace elements. *Nature Communications*, *5*. https://doi.org/10.1038/ncomms4035

Yang, X., Fan, J., & Jones, S. B. (2018). Effect of soil texture and estimate of soil-column carbon dioxide flux comparing chamber and gradient methods. *Vadose Zone Journal*, *17*(1), 180112. https://doi.org/10.2136/vzj2018.05.0112

SUPPORTING INFORMATION

Additional supporting information may be found online in the Supporting Information section at the end of the article.

How to cite this article: Alibert C, Pili E, Barre P, Massol F, Chollet S. Biologically influenced gas fluxes revealed by high-resolution monitoring of unsaturated soil columns. *Vadose Zone J*. 2020;19:e20018. https://doi.org/10.1002/vzj2.20018